FINE STRUCTURE OF THE THERMAL AND NON-THERMAL X-RAYS IN THE SN 1006 SHELL

A. Bamba[1], R. Yamazaki[1], M. Ueno[1], and K. Koyama[1]

[1]*Department of Physics, Kyoto University, Kitashirakawa, Sakyo-ku, Kyoto, 606-8502, Japan*

ABSTRACT

The North Eastern shell of SN 1006 is the most probable acceleration site of high energy electrons (up to ~ 100 TeV) with the Fermi acceleration mechanism at the shock front. We resolved non-thermal filaments from thermal emission in the shell with the excellent spatial resolution of *Chandra*. The non-thermal filaments seem thin sheets with the scales of ~ 1 arcsec (0.01 pc) and ~ 20 arcsec (0.19 pc) upstream and downstream of the shock, respectively. In a simple diffusive shock acceleration (DSA) model with the magnetic field parallel to the shock normal, the downstream region should have a highly disordered magnetic field of 30–40 μG. The width at the upstream side is extremely small, comparable to the gyro-radius of the maximum energy electrons. This result might imply that the possible scenario is not the conventional diffusive shock acceleration with a parallel magnetic field but that with a nearly perpendicular field or electron shock surfing acceleration.

INTRODUCTION

Since the discovery of cosmic rays, the origin and acceleration mechanism up to energies of $10^{15.5}$ eV (the "knee" energy) have been long-standing problems. A breakthrough came from the X-ray studies of SN 1006; Koyama et al. (1995) discovered synchrotron X-rays from the shells of this supernova remnant (SNR), indicating the existence of extremely high energy electrons up to TeV energies or more produced by the first order Fermi acceleration.

The mechanism for cosmic ray acceleration has also been studied for a long time and the most plausible process is a diffusive shock acceleration (DSA) (e.g. Bell, 1978). Apart from the globally successful picture of DSA, detailed but important processes, such as the injection and the reflection of accelerated particles, are not well understood. The spatial distribution of accelerated particles responsible for the non-thermal X-rays, may provide key information on these unclear processes. Previous observations, however, are too limited in spatial resolution for a detailed study on the structure of shock acceleration process and injection efficiency. Although many observations and theoretical models are made for SN 1006, these problems are still unsolved (e.g. Reynolds, 1998).

In this paper, we report on the first results of the spectral and spatial studies of the non-thermal shock structure in the North Eastern (NE) shell of SN 1006 with *Chandra*. We discuss the spectral analyses and determine the scale lengths of the structures for non-thermal electrons on the basis of a simple and a conventional DSA model. In this paper, we assume the distance of SN 1006 to be 2.18 kpc (Winkler et al. 2003).

OBSERVATION

We used the *Chandra* archival data of the ACIS on the NE shell of SN 1006 (Observation ID = 00732) observed on July 10–11, 2000 with the targeted position at (RA, DEC) = ($15^h03^m51^s.6$, $-41^d51^m18^s.8$). The satellite and instrument are described by Weisskopf et al. (1996). CCD chips I2, I3, S1, S2, S3, and S4 were used with the pointing center on S3. Data acquisition from the ACIS was made in the Timed-Exposure Faint mode with the readout time of 3.24 s. The data reductions and analyses were made using the *Chandra* Interactive Analysis of Observations (CIAO) software version 2.2.1. Using the Level 2 processed events provided by the pipeline processing at the *Chandra*
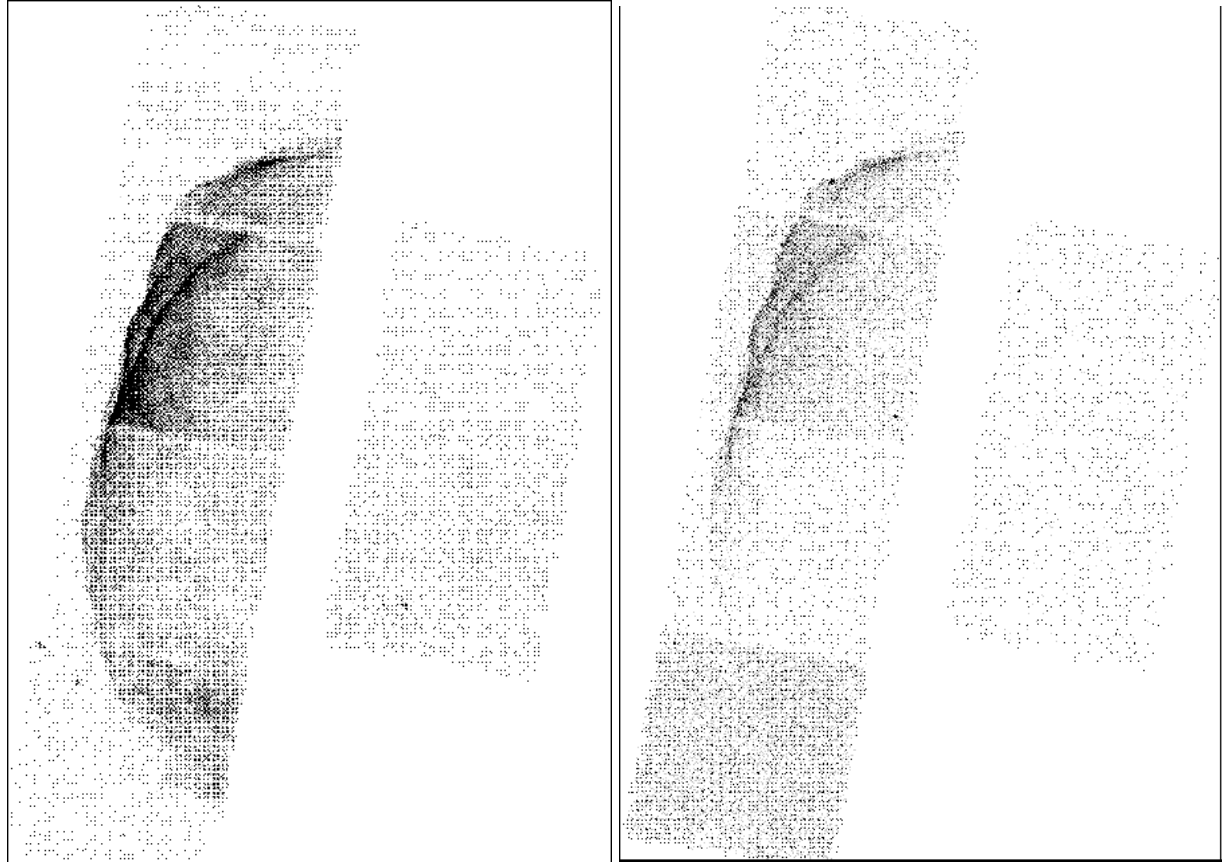
Fig. 1. The images of the North Eastern shell of SN 1006 binned with 1 arcsec scale, in the 0.5-2.0 keV band (left) and the 2.0–10.0 keV band (right), respectively, both in logarithmic scale.

X-ray Center, we selected *ASCA* grades 0, 2, 3, 4, and 6, as the X-ray events. High energy electrons due to charged particles, and hot and flickering pixels were removed. The effective exposure was ~ 68 ks for the observation. In this paper, we concentrated on the data of S3 (BI chip) because this chip has the best efficiency in soft X-rays required for the spectral analyses, and its on-axis position provides the best point-spread function required for the spatial analysis.

RESULTS

Image

Figure 1 shows the images for the NE shell of SN 1006. The images are contrasted in the 0.5–2.0 keV band (left) and in the 2.0–10.0 keV band (right) and binned to a resolution of 1 arcsec. The fine spatial resolution of *Chandra* unveils extremely narrow filaments in the hard band. They are running from north to south along the outer edge of the NE shell, parallel to the shock fronts observed by Hα emission line (Winkler and Long, 1997). The soft band image, on the other hand, has a larger scale length similar to the *ROSAT* HRI image (Winkler and Long, 1997). Many clumpy sub-structures are also seen in this energy band.

Inner Region

To resolve the thermal and non-thermal components, we made a spectrum from a bright clump found in the soft band image, which is located in the inner part of the NE shell ("Inner region" with the dashed ellipse in Figure 2). The background region was selected from a region out of the SNR, as is shown in Figure 2 with the dashed lines.

The background-subtracted spectrum can be fitted with a thin thermal plasma model in non-equilibrium ionization (NEI) state calculated by Borkowski et al. (2001) plus a power-law component. The spectrum of the inner region clump is softer than any other regions in the NE shell, which indicates that the contribution of the thermal component
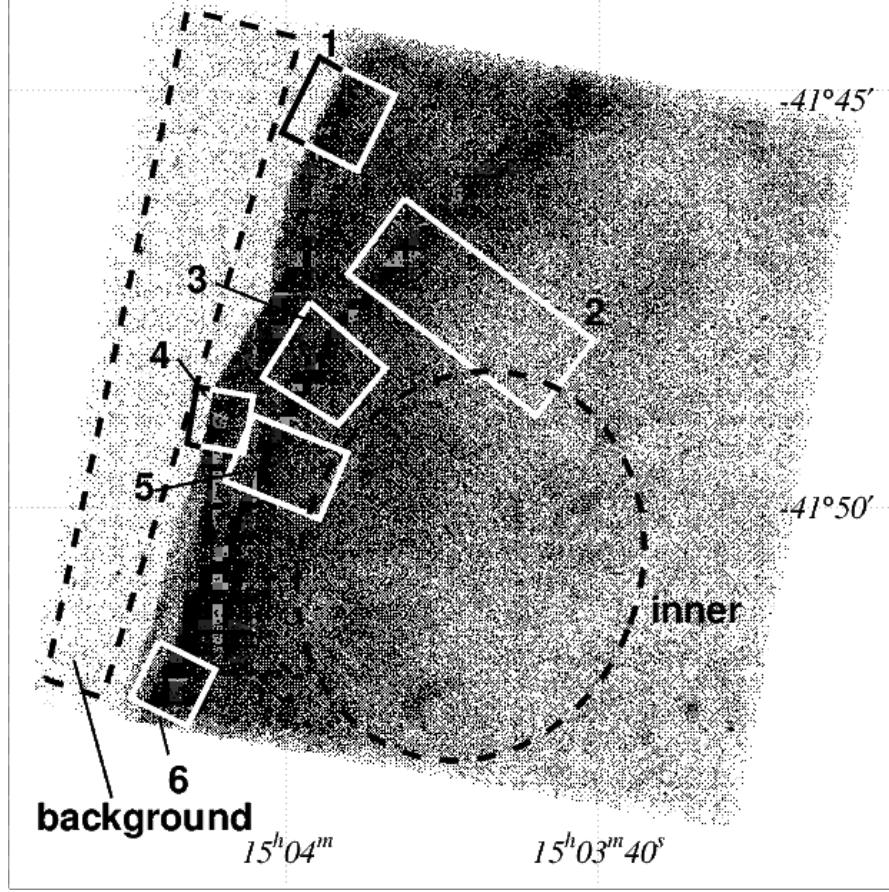
Fig. 2. The close-up view of the 0.5–10.0 keV band image. The gray scale (the left bar) is given logarithmically. The inner and background regions for the spectral analyses and the filament regions for the spatial analyses (No.1–6) are shown with dashed and solid lines, respectively.

is the largest. Nevertheless the thermal photons are only 0.02% of the non-thermal ones if we limit the energy band to 2.0–10.0 keV (the hard band). Therefore, in the following spatial analyses, we regard that all the photons in the hard band are non-thermal origin.

The Filaments

The outer edge of the NE shell is outlined by several thin X-ray filaments. For the study of these filaments, we selected 6 rectangular regions in Figure 2, in which the filaments are straight and free from other structures like superimposed filament and/or clumps. These regions (solid boxes) are shown in Figure 2 right with the designations of No.1–6 from north to south. Since the SNR shell is moving (expanding) from the right to the left, we name the right and left hand sides of the shock downstream and upstream following the standard shock physics terminology.

Figure 3 shows the intensity profiles in the hard (2.0–10.0 keV) with the spatial resolution of 0.5 arcsec, where the horizontal axis (x-coordinate) runs from the east to west (upstream to downstream) along the line normal to the filaments. To estimate the scale length, we define a simple empirical model as a function of position (x) for the profiles;

$$f(x) = \begin{cases} A \exp |\frac{x_0 - x}{w_u}| & \text{in upstream} \\ A \exp |\frac{x_0 - x}{w_d}| & \text{in downstream,} \end{cases} \tag{1}$$

where A and x_0 are the flux and position at the filament peak. We ignored the point spread function (PSF) of *Chandra* for simplicity. The scale lengths are given by w_u and w_d for upstream and downstream, respectively. The best-fit models are shown in Figure 3 with the solid lines. The mean and minimum values are 0.05 and 0.01 pc for w_u and 0.19 and 0.06 pc for w_d, respectively.
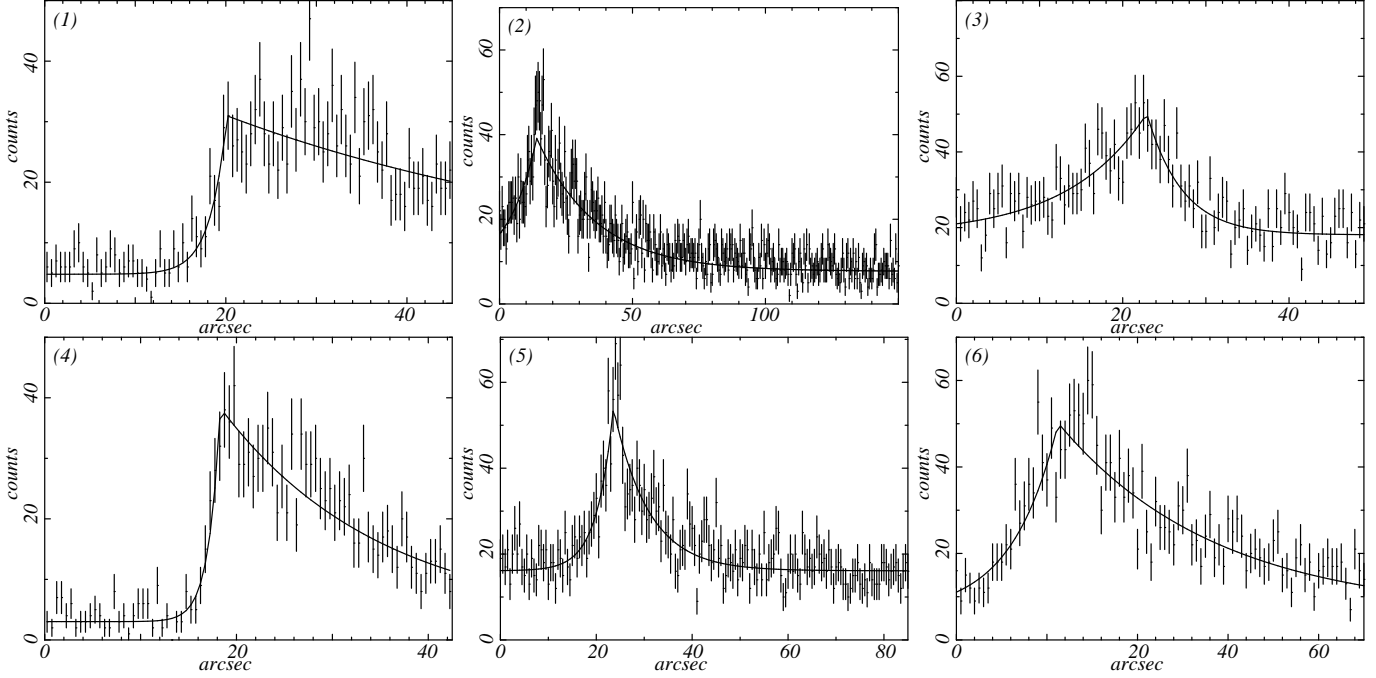
Fig. 3.　The profiles of the filaments in the North Eastern shell of SN 1006 in the 2.0–10.0 keV band.

DISCUSSION

In this section, we interpret the scale length of hard band X-rays, w_u and w_d. Blandford and Orstriker (1978) derived the distribution of accelerated particles to be flat in downstream for a steady state. However, we should consider the finite-time or energy loss effect in the SN 1006 case, where the accelerating particles must concentrate on around the shock. Therefore, we assume that the spatial distribution of non-thermal X-rays coincides with that of accelerated electrons. We consider so narrower regions than the background thermal plasma, then the magnetic field gradients can be ignored since it may be traced by the thermal emission shown in Figure 1. Here, we investigate the observed profiles based on a simple picture of DSA with the magnetic field parallel to the shock normal and a compression ratio of about 4, and estimate the physical quantities such as diffusion coefficient, magnetic field, and the maximum energy of the accelerated electrons. The scale lengths in the upstream side are the projected values of the possible sheet-like structure, hence real lengths should be smaller. Considering the PSF of *Chandra* also makes them smaller. We therefore adopted the minimum value of 0.01 pc. For the scale lengths in the downstream side, we used the mean value of 0.2 pc.

We assume that electrons emitting synchrotron X-rays are still accelerating on the shock front since the previous works suggest the magnetic field is rather small (e.g. Tanimori et al. 1998) then the effect of synchrotron radiation may be small. In this condition, the diffusion coefficients in upstream (K_u) and in downstream (K_d) are estimated from the relation $w = K/u$ as following;

$$K_u \simeq w_u \cdot u_u = w_u \cdot u_s = 8.9 \times 10^{24} \quad [\mathrm{cm^2 s^{-1}}], \tag{2}$$

$$K_d \simeq w_d \cdot u_d = w_d \cdot \frac{1}{4} u_s = 4.2 \times 10^{25} \quad [\mathrm{cm^2 s^{-1}}], \tag{3}$$

where the shock speed u_s is assumed to be 2890 km s^{-1} (Winkler et al. 2003). The acceleration time scale τ_{acc} is then $\tau_{acc} = \frac{4}{u_s^2}(K_u + 4K_d)$ (Drury 1983);

$$\tau_{acc} \simeq 8.6 \times 10^9 \ [\mathrm{sec}] \ = 270 \ [\mathrm{years}] \tag{4}$$

The energy loss time scale (τ_{loss}) via synchrotron cooling should be longer than the acceleration time scale of about
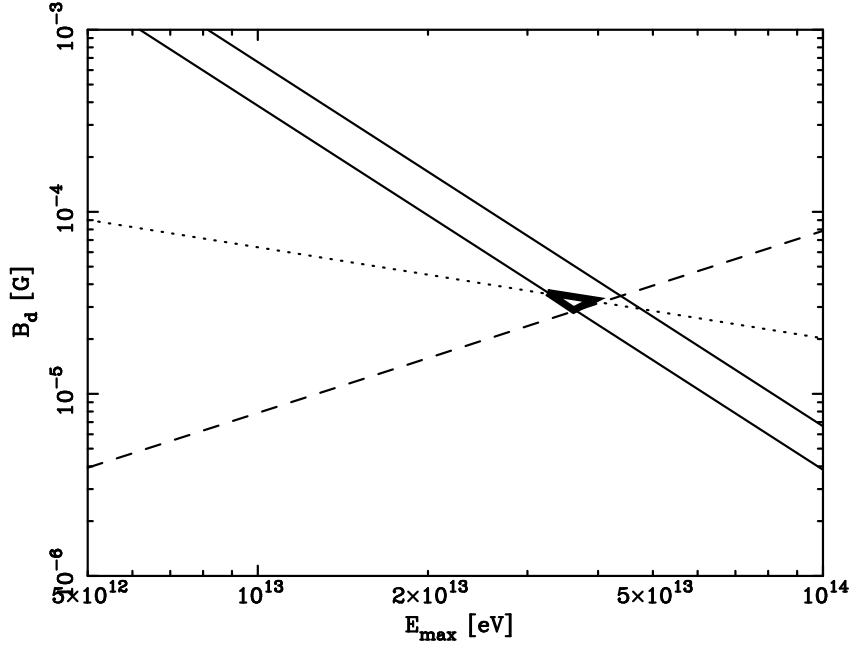
Fig. 4. The relation between E_{max} and B_d. The solid, dotted, and dashed lines are the relation derived from $E_{rolloff}$, acceleration time scale, and Bohm limit in the filaments. The thick line region is the most probable region for E_{max} and B_d.

300 year, hence using Eq. (4), we obtain;

$$6.3 \times 10^2 B_d^{-2} E_{max}^{-1} \geq 8.6 \times 10^9 \quad [\text{sec}] \tag{5}$$

A probable region in the $E_{max}-B_d$ space is then limited to the lower side of the dotted line in Figure 4.

The wide band spectra from X-ray to radio can be fitted with the *srcut* model (Reynolds, 1998). The best-fit $\nu_{rolloff}$ at the filaments is 2.6 (1.9–3.3)$\times 10^{17}$ Hz, which constrains the maximum energy of electrons E_{max} and downstream magnetic field B_d;

$$E_{max} B_d^{0.5} = 0.37^{+0.04}_{-0.06} \quad [\text{ergs G}^{0.5}] \tag{6}$$

The allowed region in the $E_{max}-B_d$ plane is between the two solid lines of Figure 4.

The downstream diffusion coefficient is given by Skilling (1975) as follows;

$$K_d = \frac{1}{3}\xi_d \frac{E_{max}}{e B_d} c, \tag{7}$$

where ξ is a non-dimensional parameter depending on the angle between the shock normal and the upstream magnetic field θ and the gyro factor η, which is the ratio of the mean free path of particles along the magnetic field to their gyro radius (Jokipii, 1987). Since we consider the case of $\theta = 0$, ξ_d must be η_d and larger than 1. The dashed line in Figure 4 is the relation of Eq. (7) for $\xi_d = 1$ (Bohm limit). Therefore, a probable region in the $E_{max}-B_d$ space is to the upper of the dashed line.

Using Eq. (5), (6), and (7), we thus constrain the most likely region in the $E_{max}-B_d$ space to be in between the thick lines, where the magnetic field in downstream (B_d) and the maximum electron energy (E_{max}) are in the range of 30–40 μG and 30–40 TeV, respectively. The small ξ_d (the likely region is $1 \leq \xi_d \leq 1.6$) indicates that the magnetic field is highly turbulent. Figure 4 also suggests that the synchrotron loss time scale is nearly equal to the acceleration one and electrons begin to loss their energy.

From Eq. (7), the ratio of the diffusion coefficient ($\frac{K_u}{K_d}$) is given by $\frac{\xi_u B_d}{\xi_d B_u}$. Observationally, the ratio is about 0.2 (from Eq. (2) and (3)), we thus obtain the relation of magnetic field and ξ between upstream and downstream as

$$\frac{\xi_u}{\xi_d} \sim 0.2 \frac{B_u}{B_d} \tag{8}$$

Since $\frac{B_u}{B_d} = 1$ with $\theta = 0$, and considering the large errors and many assumptions, we find that $\xi_u = \eta_u$ may be marginally acceptable only near to 1, while it might exist that other possible scenarios explaining observed thin filaments. For example, the "apparent" diffusion coefficients in upstream can be extremely small in the case of a nearly perpendicular magnetic field in this region as suggested by Jokipii (1987).

In this paper, we assumed the age-limited case. On the other hand, Figure 4 shows that the cooling process might be important and that we might have to consider the cooling-limited case. In such a case, protons might be accelerated to higher energy than electrons. This case is under investigation (Yamazaki et al. 2003).

Our constraint is more strict than determined from radio data by Achterberg et al. (1994), because the spatial resolution of *Chandra* is better than their data and the diffusion length determined by X-rays must be larger than that determined by radio. Since the current radio polarization data are spatially poor and limited mainly to the downstream region, fine structure observations, particularly at the very narrow region in the upstream side should be crucial. Of course our result is derived in a very indirect way with the many assumptions, and as a result has large uncertainty, then the DSA process might be able to explain marginally the observed results even in parallel magnetic field. However, we point out that another acceleration mechanism may be able to explain our results, the thin non-thermal filaments. For example, Hoshino and Shimada (2002) proposed the electron shock surfing acceleration mechanism. More quantitative study is necessary, whether the mechanism can accelerate particles up to 30 TeV in this system and whether the accelerated particles have the power-law spectrum.

ACKNOWLEDGEMENTS

REFERENCES

Achterberg, A., Blandford, R.D., and Reynolds, S.P., Evidence for enhanced MHD turbulence outside sharp-rimmed supernova remnants, Astron. Astrophys., 281, 220–230, 1994.

Bell, A.R., The acceleration of cosmic rays in shock fronts. II, Mon. Not. R. Astron. Soc., 182, 443–455, 1978.

Blandford, R.D., and Orstriker, J.P., Particle acceleration by astrophysical shocks, Astrophys. J., 221, L29–L32, 1978.

Borkowski, K.J., Lyerly, W.J., and Reynolds, S.P., Supernova remnants in the Sedov expansion phase: thermal X-ray emission, Astrophys. J., 548, 820–835, 2001.

Drury, L.O'C., An introduction to the theory of diffusive shock acceleration of energetic particles in tenuous plasmas, Rep. Prog. Phys., 46, 973–1027, 1983.

Hoshino M., and Shimada N., Nonthermal electrons at high mach number shocks: electron shock surfing acceleration, Astrophys. J., 572, 880–887, 2002.

Jokipii, J.R., Rate of energy gain and maximum energy in diffusive shock acceleration, Astrophys. J., 313, 842, 1987.

Koyama, K., Petre, R., Gotthelf, E.V., Hwang, U., Matsura, M., Ozaki, M., and Holt S.S., Evidence for shock acceleration of high-energy electrons in the supernova remnant SN 1006, Nature, 378, 255–258, 1995.

Reynolds, S.P., Models of synchrotron X-rays from shell supernova remnants, Astrophys. J., 493, 375–396, 1998.

Skilling, J., Cosmic ray streaming. I - Effect of Alfven waves on particles, Mon. Not. R. Astron. Soc., 172, 557–566, 1975.

Tanimori, T., Hayami, Y., Kamei, S. et al., Discovery of TeV gamma rays from SN 1006: Further evidence for the supernova remnant origin of cosmic rays, Astrophys. J., 497, L25–L28, 1998.

Weisskopf, M.C., O'dell, S.L., and van Speybroeck, L.P., Advanced X-ray astrophysics facility (AXAF), *Proc. SPIE*, 2805, 2–7, 1996.

Winkler, P.F. and Long, K.S., X-ray and optical imagery of the SN 1006 supernova remnant, Astrophys. J., 491, 829–838, 1997.

Winkler, P. F., Gupta, G., and Long, Knox S., The SN 1006 remnant: Optical proper motions, deep imaging, distance, and brightness at maximum, Astrophys. J., 585, 324–335, 2003.

Yamazaki, R., Yoshida, T., Terasawa, T., Bamba, A., Ueno, M., and Koyama, K., Constraints on the diffusive shock acceleration from the nonthermal X-ray thin shells in SN 1006 NE rim, submitted to A&A

E-mail address of A. Bamba: bamba@cr.scphys.kyoto-u.ac.jp